Support Information

For

Theoretical study of water adsorption and dissociation on Ta_3N_5 (100) surfaces

Submitted to ***Physical Chemistry Chemical Physics***

by

Jiajia Wang[a], Wenjun Luo[a], Jianyong Feng[a], Li Zhang[a], Zhaosheng Li[a*] and Zhigang Zou[a,b*]

[a)]National Laboratory of Solid State Microstructures, Department of Physics, Ecomaterials and Renewable Energy Research Center (ERERC), and College of Engineering and Applied Sciences, Nanjing University, 22 Hankou Road, Nanjing 210093, People's Republic of China.

[b)]Key Laboratory of Atmospheric Environment Monitoring and Pollution Control, Nanjing University of Information Science and Technology, People's Republic of China.

[*]Corresponding Authors: Tel: +86-25-83686630, Fax: +86-25-83686632, E-mail: zsli@nju.edu.cn or zgzou@nju.edu.cn

SI-1 Crystal structures and electronic structures of the bulk Ta_3N_5

The atomic model of bulk Ta_3N_5 is shown in Fig. S1a. In Ta_3N_5, the Ta atom is coordinated with six neighboring N atoms, while N atoms are coordinated with three (N3) or four (N4) Ta atoms[1]. Based on the GGA-PBE computational scheme, our relaxed lattice constants of conventional Ta_3N_5 cell are a=3.91, b=10.32 and c=10.35 Å, which agrees well with the experimental (experimental lattice constants[2]: a=3.8862, b=10.2118, c=10.2624 Å) and other theoretical results[3,4]. The band structure of bulk Ta_3N_5 shown in Fig. S1b reveals that, Ta_3N_5

is an indirect gap semiconductor with VBM and CBM locating at Γ and Y points, respectively. Our calculated band gap (1.27 eV) is smaller than the experimental result (2.1 eV), which is ascribed to the gap underestimation of the GGA method[5,6]. A prominent character of band structure of Ta_3N_5 is the delocalization of the conduction band. Since electron and hole in delocalized band have lighter effective masses[7], photo-excited electron in the conduction band of Ta_3N_5 is expected to have excellent mobility, thus facilitating segregation of electron-hole pairs. The partial density of states (PDOS) of the bulk Ta_3N_5 is shown in Fig. S1c. As can be seen, the valence band and conduction band of Ta_3N_5 mainly consist of N2p and Ta5d orbital, respectively. Our calculated electronic structures of bulk Ta_3N_5 are in good agreement with other theoretical reports[3,4].

SI-2 Chemical potentials of N, O and Ta in Ta_3N_5

Under thermal equilibrium growth conditions, Ta_3N_5 should satisfy:

$$3\mu_{Ta} + 5\mu_N = E^f_{Ta_3N_5} = -8.47eV \quad \text{(S1)}$$

where $E^f_{Ta_3N_5}$ is the formation energy of pure Ta_3N_5 which agrees with other theoretical value[8] (-9.45 eV) based on the Hybrid density-functional calculation method. Then, μ_N and μ_{Ta} under different growth conditions can be determined: under N-poor (Ta-rich) growth condition, μ_N =-1.69 and μ_{Ta} =0 eV; under N-rich (Ta-poor) growth condition, μ_N = 0 and μ_{Ta} =-2.82 eV. To determine the value of μ_O, precipitation of secondary phases such as TaON and Ta_2O_5 should be avoided:

$$\mu_N + \mu_O + \mu_{Ta} < E^f_{TaON} = -5.79eV \quad \text{(S2)}$$

$$5\mu_O + 2\mu_{Ta} < E^f_{Ta2O5} = -20.20eV \quad \text{(S3)}$$

where $E^f_{Ta_2O_5}$ and E^f_{TaON} are the formation energies of Ta_2O_5 and TaON, respectively. Our calculated formation energies of Ta_2O_5 and TaON agree with that in other theoretical reports[8] (-6.23 eV and -18.14 eV for Ta_2O_5 and TaON, respectively). Then, μ_O can be calculated from the lower bound for each growth condition: -4.10 and -2.97 eV under N-poor/Ta-rich and N-rich/Ta-poor growth conditions, respectively.

SI-3 The S_{bottom} term

The S_{bottom} is defined as:

$$S_{bottom} = (E_{slab} - n_N\mu_N - n_{Ta}\mu_{Ta})/(2A) \quad \text{(S4)}$$

where n_i and μ_i (i=N, Ta) are the number and chemical potential of N and Ta, respectively, and A (106.81 $Å^2$) is the surface area of the slab model. Note that, the E_{slab} term in the above equation is calculated by using of the PERFECT Ta_3N_5 (100) surface model WITHOUT any geometry relaxation. Since the two sides of this non-relaxed Ta_3N_5 (100) surface model are completely identical, the term "2" should be divided. In geometry relaxation of the perfect, oxygen containing and nitrogen vacancy containing Ta_3N_5 (100) surfaces, the two bottom atomic layers are fixed while other layers are allowed relaxation. After geometry relaxation, the bottom surface is different from the top surface, and thus surface energy of the bottom surface is also different from that of the top surface. Therefore, to obtain the surface energy of the top surface, which is exactly what we really concern, the surface energy of the bottom surface, i.e., the S_{bottom}, must be subtracted.

We used to calculate surface energies of the perfect, oxygen containing and nitrogen vacancy containing Ta_3N_5 (100) surfaces using the symmetry slab model. This symmetry slab

model is constructed with eleven Ta_6N_{10} atomic layers. In the process of geometry relaxations, the central Ta_6N_{10} atomic layer is fixed while the rest five Ta_6N_{10} atomic layers on each side of the slab model are allowed to relax. The calculated surface energies using the symmetry slab model are listed in the Table S1. As can be seen, the surface energies calculated by the symmetry slab model are in good agreement with that by the non-symmetry seven atomic Ta_6N_{10} atomic layers used in this study. Therefore, the seven atomic Ta_6N_{10} atomic layers is sufficient to simulate the Ta_3N_5 (100) surfaces.

SI-4 Less stable adsorption models for water adsorption on the perfect Ta_3N_5 (100) surface

For water adsorption on the perfect Ta_3N_5 (100) surface, a lot of initial water adsorption models have been optimized. The $[100]_{mol}$ and $[100]_{dis}$ models are just the most stable structures for molecular and dissociative water adsorptions, respectively. Actually, molecular and dissociative water adsorptions can also be found in other optimized models, although these models are less stable because of their higher adsorption energies compared with $[100]_{mol}$ and $[100]_{dis}$ models. Here, we present two less stable adsorption models which are denoted as $[100]_{mol(less)}$ and $[100]_{dis(less)}$. In the main manuscript, both the $[100]_{mol}$ and $[100]_{dis}$ models are optimized with H atoms of the water molecule initially bonding to $N4_{top}$ atoms, while $[100]_{mol(less)}$ and $[100]_{dis(less)}$ models are optimized with H atoms initially bonding to $N3_{top}$ atoms. The optimized structures and adsorption energies for $[100]_{mol(less)}$ and $[100]_{dis(less)}$ models are shown in Fig. S2. It is seen that, for the $[100]_{mol(less)}$ model, water is molecularly adsorbed onto the surface with O_w bonding to Ta_{top} atom. For the $[100]_{dis(less)}$ model, water is

decomposed with O_wH_a bonding to Ta_{top} atom and H_b bonding to $N3_{top}$ atom.

SI-5 The Mulliken charge analysis for water adsorption surface models

Since the VASP code can only calculate the Bader charge, we choose the Castep[9] code to make the Mulliken[10] analysis. The exchange correlation potential is described by the GGA-PBE scheme. The cutoff energy is 340 eV. We do not use the Castep code to make geometry relaxation for each water adsorbed model, because geometry relaxation using the Castep code costs a lot time. Then, we simply use the optimized structure obtained from the VASP code to make the Mulliken analysis by the Castep code.

The Bader charge calculated by the VASP code and the Mulliken charge calculated by the Castep code are shown in Table S2. For both the Bader charge and Mulliken charge, the positive and negative values mean acceptance and donation of electron for the water, respectively. As can be seen, for most surface models, the number of donated or accepted electrons calculated by the Bader charge is bigger than that calculated by the Mulliken charge. This is consistent with the reported order of Bader and Mulliken charge[11]: Bader > Mulliken (Note that, in reference 11, the Bader charge is denoted as AIM). However, the relative difference among different surface models calculated by the Bader charge is nearly the same as that calculated by the Mulliken charge. For example, for both Bader and Mulliken analysis, the charge of water dissociative adsorption model is always bigger than that of the molecular adsorption model. Furthermore, for both Bader and Mulliken analysis, the charge order of perfect, oxygen containing and nitrogen vacancy containing surface models is perfect < oxygen containing < nitrogen vacancy containing. Therefore, comparisons between the Bader

and Mulliken analysis reveal that our calculated Bader charge is reasonable and reliable.

SI-6 Less stable adsorption models for water adsorption on the oxygen containing Ta_3N_5 (100) surface

According to the coordination environment and position of N atom on the Ta_3N_5 (100) surface, nitrogen atoms $N3_{top}$, $N4_{top}$ and $N3_{sub}$ can be substituted with O_{surf} atom, leading to three oxygen containing Ta_3N_5 (100) surfaces. The $[100+O_{surf}]_{mol}$ and $[100+O_{surf}]_{dis}$ models have been presented in the main manuscript corresponding to the most stable molecular and dissociative adsorption models, respectively. In $[100+O_{surf}]_{mol}$ and $[100+O_{surf}]_{dis}$ models, the O_{surf} atom substitutes for $N4_{top}$ and $N3_{top}$ atoms, respectively. As we have stated in SI-4, molecular and dissociative water adsorptions can also be found in optimization of other initial models. Then, in this section, we present three less stable adsorption models which are denoted as $[100+(O_{N4})_{top}]_{dis}$, $[100+(O_{N3})_{top}]_{mol}$ and $[100+(O_{N3})_{sub}]_{mol}$. The $[100+(O_{N4})_{top}]_{dis}$ model is a dissociative water adsorption with O_{surf} substitution for $N4_{top}$ atom. The $[100+(O_{N3})_{top}]_{mol}$ and $[100+(O_{N3})_{sub}]_{mol}$ models are both molecular water adsorptions with O_{surf} substitution for $N3_{top}$ and $N3_{sub}$ atoms, respectively. The optimized structures and adsorption energies for these three models are shown in Fig. S3.

It is seen that, in the $[100+(O_{N4})_{top}]_{dis}$ model, water is decomposed to O_wH_a and H_b, with O_wH_a bonding to Ta_{top} atom and H_b bonding to $N4_{top}$ atom, respectively. The adsorption sites for water in the $[100+(O_{N4})_{top}]_{dis}$ is the same as that in the $[100+O_s]_{dis}$ model. In the $[100+(O_{N3})_{top}]_{mol}$ model, water is molecularly adsorbed with O_w bonding to Ta_{top} atom and two H atoms locating above two surface $N4_{top}$ atoms. The $[100+(O_{N3})_{sub}]_{mol}$ model is

optimized with water initially locating above the sub-surface. After geometry optimization, we found that the water leaves away from the sub-surface and molecularly adsorbs on the top-surface, with O_w bonding to Ta_{top} atom and two H atoms locating above two $N4_{top}$ atoms. The adsorption sites for molecular water adsorption in the $[100+(O_{N3})_{sub}]_{mol}$ is the same as that in the $[100+(O_{N3})_{top}]_{mol}$, leading to the nearly same adsorption energies for these two models.

SI-7 Results of water adsorption on the Ta_3N_5 (100) surface with $(V_{N4})_{top}$

The optimized structure, denoted as $[100+(V_{N4})_{top}]_{mol}$, and adsorption energy of water adsorption on the Ta_3N_5 (100) surface with $(V_{N4})_{top}$ are shown in Fig. S4. The water molecule is initially put in the $(V_{N4})_{top}$ site with different directions. As can be seen, after structural optimization, the water is molecularly adsorbed near the $(V_{N4})_{top}$ site.

References

1 S. J. Henderson and A. L. Hector, *J. Solid State Chem.*, 2006, **179**, 3518-3524.

2 N. E. Brese, M. O'Keeffe, P. Rauch and F. J. DiSalvo, *Acta Crystallogr., Sect. C*, 1991, **47**, 2291-2294.

3 C. M. Fang, E. Orhan, G. A. de Wijs, H. T. Hintzen, R. A. de Groot, R. Marchand, J. Y. Saillard and G. de With, *J. Mater. Chem.*, 2001, **11**, 1248-1252.

4 E. Watanabe, H. Ushiyama and K. Yamashita, *Chem. Phys. Lett.*, 2013, **561-562**, 57-62.

5 J. P. Perdew and M. Levy, *Phys. Rev. Lett.*, 1983, **51**, 1884-1887.

6 L. J. Sham and M. Schluter, *Phys. Rev. Lett.*, 1983, **51**, 1888-1891.

7 Z. Y. Zhao, W. J. Luo, Z. S. Li and Z. G. Zou, *Phys. Lett. A*, 2010, **374,** 4919-4927.

8 S. Y. Chen and L. W. Wang, *Appl. Phys. Lett.*, 2011, **99**, 222103.

9 R. S. Mulliken, *J. Chem. Phys.*, 1955, **23**, 1833-1840.

10 M. D. Segall, Philip J. D. Lindan, M. J. Probert, C. J. Pickard, P. J. Hasnip, S. J. Clark and M. C. Payne, *J. Phys.: Condens. Mater.*, 2002, **14**, 2717-2744.

11. F. De Proft, C. Van Alsenoy, A. Peeters, W. Langenaeker and P. Geerlings, *J. Comput. Chem.*, 2002, **23**, 1198-1209.

Table S1. Surface energies of the perfect Ta_3N_5 (100) surface and Ta_3N_5 (100) surface with different surface defects such as $(V_{N3})_{top}$, $(V_{N4})_{top}$, $(O_{N3})_{top}$ and $(O_{N4})_{top}$ calculated using the non-symmetry and symmetry slab surface models. Surface energies under two grow conditions, N-poor (Ta-rich) and N-rich (Ta-poor), are shown.

Slab model	Growth condition	Surface energies (J/m^2)				
		perfect	$(V_{N3})_{top}$	$(V_{N4})_{top}$	$(O_{N3})_{top}$	$(O_{N4})_{top}$
non-symmetry	N-poor	1.22	1.10	1.26	1.10	1.13
	N-rich	1.22	1.35	1.52	1.19	1.22
symmetry	N-poor	1.22	1.09	1.26	1.10	1.13
	N-rich	1.22	1.35	1.52	1.19	1.22

Table S2. Bader charge calculated by the VASP code and the Mulliken charge calculated by the Castep code for different water adsorption models

Models	Bader	Mulliken
$[100]_{mol}$	-0.03	-0.01
$[100]_{dis}$	0.13	0.08
$[100+O_{surf}]_{mol}$	-0.05	-0.03
$[100+O_{surf}]_{dis}$	0.13	0.08
$[100+(V_{N3})_{top}]_{mol}$	0.01	0.03
$[100+(V_{N3})_{top}]_{dis}$	1.18	0.76
$[100+(V_{N3})_{sub}]_{mol}$	0.02	0.00
$[100+(V_{N3})_{sub}]_{dis}$	1.22	0.79

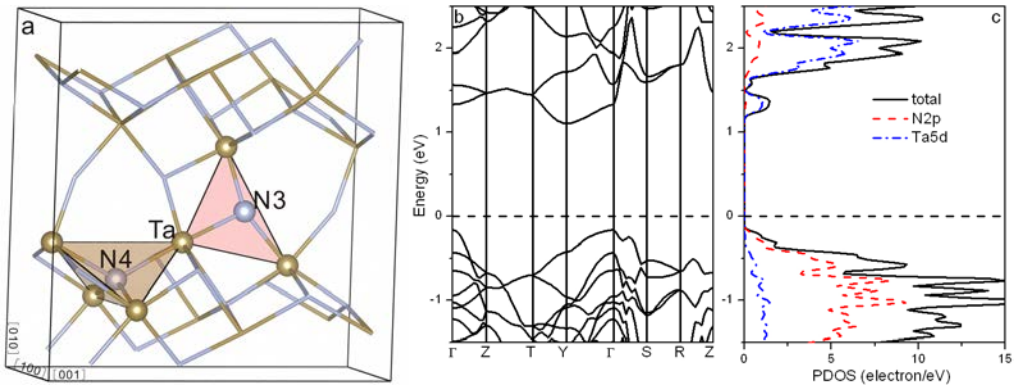

Fig. S1. (Colour online) (a) Unit cell of conventional bulk Ta_3N_5. The yellow and grey balls are Ta and N atoms, respectively. (b) and (c) are the band structure and partial density of states (PDOS) of bulk Ta_3N_5, respectively. Vertical dash lines are the Fermi energy level.

side-view top-view

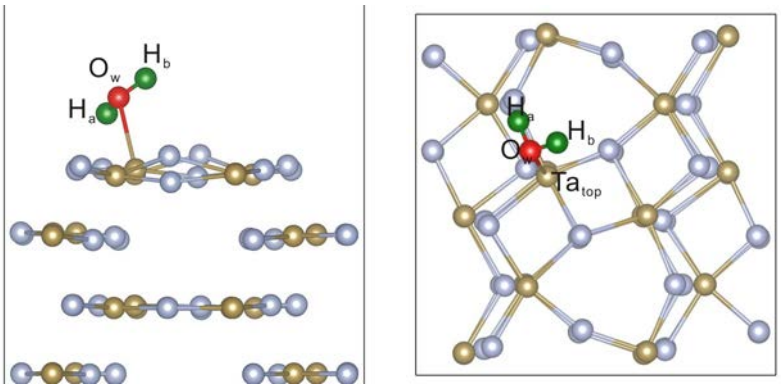

(a) $[100]_{mol(less)}$: $d(H_a\text{-}O_w)$= 1.03 Å; $d(H_b\text{-}O_w)$= 0.98 Å; ∠H_a-O_w-H_b=107.80 degree; E_{ads}=0.09 eV

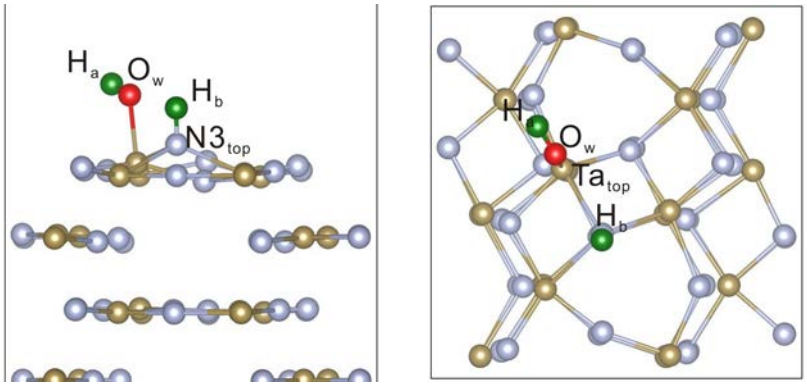

(b) $[100]_{dis(less)}$: $d(H_a\text{-}O_w)$= 0.97 Å; $d(H_b\text{-}O_w)$= 2.74 Å; ∠H_a-O_w-H_b=168.30 degree; E_{ads}=-1.69 eV

Fig. S2. Optimized structures and adsorption energies for (a) $[100]_{mol(less)}$ and (b) $[100]_{dis(less)}$ models (b)

side-view top-view

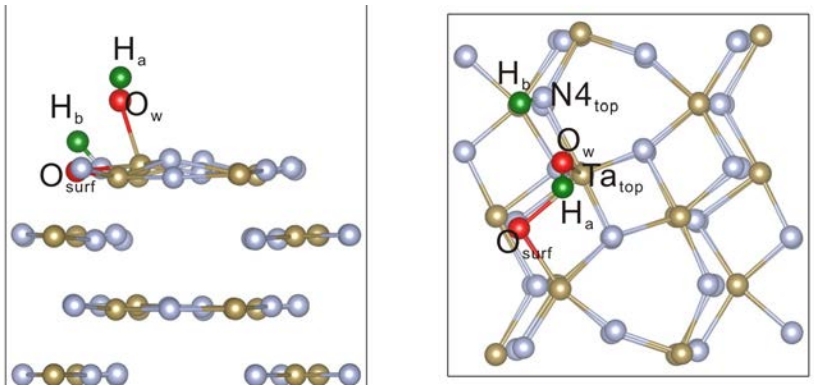

(a) $[100+(O_{N4})_{top}]_{dis}$: $d(H_a\text{-}O_w)$= 0.97 Å; $d(H_b\text{-}O_w)$= 2.39 Å; $\angle H_a\text{-}O_w\text{-}H_b$=149.19 degree; E_{ads}=-1.70 eV

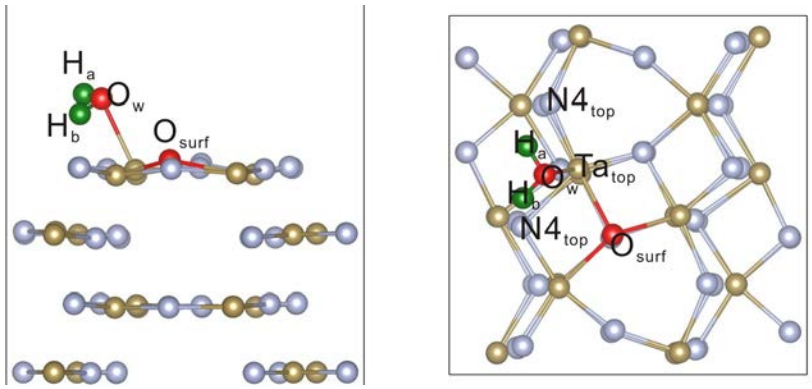

(b) $[100+(O_{N3})_{top}]_{mol}$: $d(H_a\text{-}O_w)$= 0.98 Å; $d(H_b\text{-}O_w)$= 1.00 Å; $\angle H_a\text{-}O_w\text{-}H_b$=107.37 degree; E_{ads}=-0.94 eV

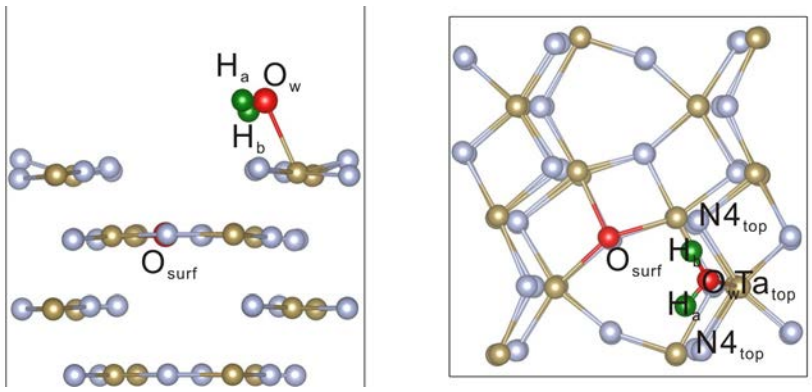

(c) $[100+(O_{N3})_{sub}]_{mol}$: $d(H_a\text{-}O_w)$= 0.98 Å; $d(H_b\text{-}O_w)$= 1.02 Å; $\angle H_a\text{-}O_w\text{-}H_b$=107.31 degree; E_{ads}=-0.90 eV

Fig. S3. Optimized structures and adsorption energies for (a) $[100+(O_{N4})_{top}]_{dis}$ (b) $[100+(O_{N3})_{top}]_{mol}$ and (c) $[100+(O_{N3})_{sub}]_{mol}$ models.

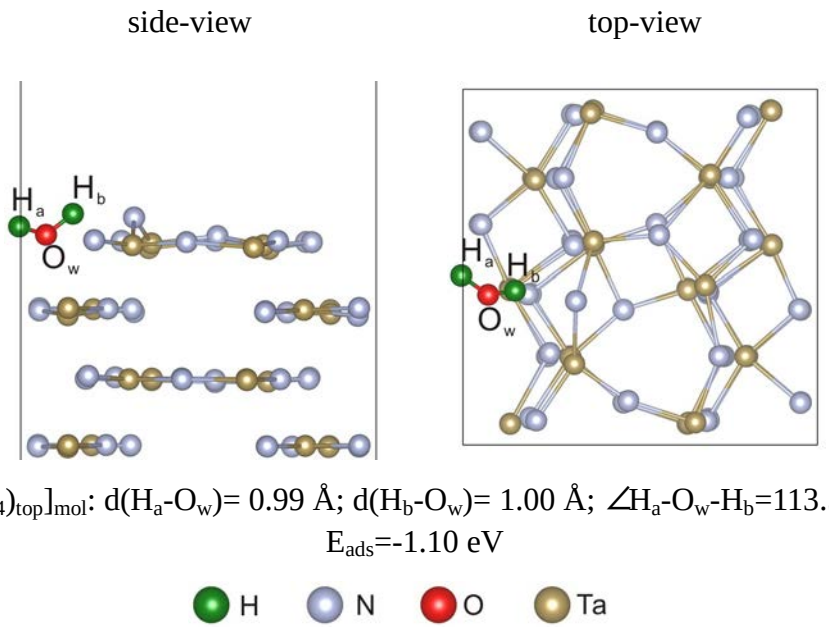

Fig. S4. Optimized structures and adsorption energies for the $[100+(V_{N4})_{top}]_{mol}$ model.